Synthesis and characterization of TiO_2: Evaluation for possible application as light trapping layer in thin film solar cells

R. Jaffar*, C. Donga, L.E. Mathevula and P.S. Mbule*

Department of Physics, CSET, University of South Africa, Johannesburg, 1710, South Africa

*E-mail: rjaffar6424397@gmail.com and mbuleps1@unisa.ac.za

Abstract

In this study, titanium dioxide (TiO_2) nanoparticles (NPs) were synthesized using the sol–gel method for a 2 hr reaction time and thereafter modified to evaluate their effects on the performance of perovskite-based solar cells (PSCs). The synthesized NPs were then annealed at 500°C for 3 hr. Structural, morphological, compositional, and optical characterization was carried out using X-ray diffraction (XRD), Raman spectroscopy, scanning electron microscopy (SEM) and UV-Vis diffuse reflectance spectroscopy. The XRD patterns confirmed the crystalline nature and tetragonal structure of the TiO_2 NPs while the average crystallite size and dislocation line density were estimated using the Debye–Scherrer relation. The average crystallite size decreased from 4.75 nm before annealing to 3.69 nm after annealing while the dislocation density increased from 0.01×10^{15} to 0.245×10^{15} lines/m². Raman spectroscopy further validated the presence of the anatase phase through peak analysis. The presence of sharp and intense Raman peaks indicates improved crystallinity and reduced structural disorder after annealing. SEM analysis revealed increased grain size and improved particle uniformity. UV–Vis analysis showed absorption in the range of 390–450 nm. After annealing, the band gap values slightly decreased from 2.85 to 2.73 eV. The SCAPS-1D software was further used to simulate the possible power conversion efficiency (PCE) of the proposed PSC device. The simulated device achieved higher PCE values of 25.71% and 24.42% from unannealed and annealed TiO_2 NPs, respectively.

1. Introduction

Perovskite solar cells (PSCs) have drawn a lot of interest because of their superior optoelectronic characteristics, which include low recombination losses, high absorption coefficients and effective charge transport. The most promising of these are organic–inorganic lead halide perovskites, which have excellent charge carrier mobility, strong light absorption and efficient exciton mobility. All of these parameters contribute significantly to the high power conversion efficiencies (PCEs) achieved by PSCs [1]. Since their introduction by Kojima et al. in 2009, PSCs have rapidly advanced, with methyl ammonium lead iodide ($CH_3NH_3PbI_3$)-based devices now achieving PCEs exceeding 25%, making them competitive with conventional silicon-based solar cells[2] Ongoing research has focused on improving the performance, stability, and scalability of PSCs by modifying the perovskite layer and other device components**.** The electron transport layer (ETL) is one of the layers that is most important for charge extraction and overall device efficiency. The superior optical and electrical properties, good energy level alignment, and chemical stability of titanium dioxide (TiO_2) make it one of the most used ETL materials in PSCs. Particularly TiO_2 nanoparticles (NPs) have a large surface area, which makes them perfect for solar applications[3]**.** In this work the characteristics of TiO_2 NPs have been evaluated experimentally. Additionally, a modified planar n–i–p architecture (ITO/TiO_2/$CH_3NH_3PbI_3$/Spiro-OMeTAD/Au) is investigated using SCAPS-1D simulation to determine the impact of TiO_2 NPs optimization on device performance**.**

2. Experimental

2.1 Sol-gel synthesis of TiO_2 NPs

Titanium tetraisopropoxide (TTIP, 97%), isopropanol (70% in aqueous solution), nitric acid (70%) and deionized water were utilized to synthesize (TiO_2 NPs) by the sol-gel method. 5 mL of TTIP was slowly added to 6 mL of isopropanol under continuous stirring at room temperature and the mixture was stirred for 15 min. 75 mL of deionized water was gradually introduced, forming a white precipitate that quickly transformed into a white solution. The mixture was heated and stirred at 80–85°C for 1 h. Subsequently, 2.5 mL of nitric acid was added dropwise with constant stirring, followed by continued heating for 2 more hr to induce peptization. After cooling to room temperature the solution was oven-dried at 60–65°C for 6 hr and 30 min. The dried NPs were ground into a fine powder and annealed at 500°C for 3 hr to improve crystallinity. Figure 1(a) and (b) illustrate the preparation method and the proposed PSC device configuration.

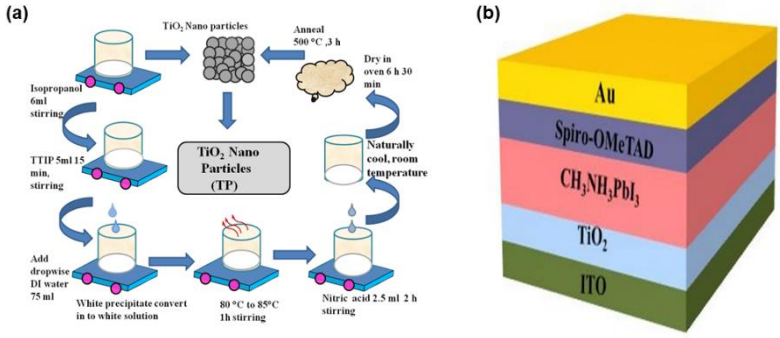

Figure 1. (a) A schematic representation of the sol–gel synthesis for TiO_2 nanoparticles and (b) the proposed device configuration under AM1.5G illumination (1000 W/m^2)

2.2 PSC Device Simulation using SCAPS-1D

The continuity and Poisson's equations were used to simulate the PSC device using SCAPS-1D software. The continuity equations explain how electrons and holes behave in the device, while Poisson's equation explains the electric potential caused by the distribution of charges. These are shown by equations 1 to 3[4]

$$\nabla^2\psi = q/\varepsilon(\mathrm{n} - \mathrm{p} + \mathrm{N_A} - \mathrm{N_D}) \quad (1)$$

$$\nabla J_n - q\frac{\partial n}{\partial t} = +qR \quad (2)$$

$$\nabla J_P + q\frac{\partial p}{\partial t} = -qR \quad (3)$$

where ψ represents the electric potential, n and p denote the densities of electrons and holes respectively, while N_A and N_D correspond to the concentrations of acceptors and donors. The symbol q signifies the charge of an electron, and ε indicates the dielectric constant of the materials involved. Jn and Jp represent the current densities of electrons and holes and R denotes the rate of recombination.Figure1(b)show the proposed architecture of the (PSC), which has been simulated using SCAPS with a lead-based perovskite absorber, specifically ($CH_3NH_3PbI_3$), acknowledged for its advantageous properties and enhanced efficiency, with Spiro-OMeTAD functioning as the hole transport layer. The device configuration is as follows: ITO/TiO_2/$CH_3NH_3PbI_3$/Spiro-OMeTAD/Au. Incident light is transmitted through the indium tin oxide (ITO) front contact, with TiO_2 NPs serve as the light trapping and electron transport layer (ETL), $CH_3NH_3PbI_3$ functioning as the light absorber, Spiro-OMeTAD designated as the hole transport layer (HTL), and gold (Au) designated as the rear contact. Simulations were run at 300 K with AM 1.5 G illumination (1000 W/m²). TiO_2 NPs having band gap values of 2.85 eV and 2.73 eV, respectively, were used to compare two models before and after annealing at 500°C [5].

3. Results and discussion

3.1 X-ray diffraction (XRD) analysis

The XRD patterns of TiO_2 NPs in the 2θ range of (20–70°) are shown in Figure 2(a), confirming good crystallinity, phase purity and structural information. XRD peaks of TiO_2 NPs the diffraction peaks match well with anatase phases of TiO_2 NPs. The main peaks at 25.21°, 37.80°, 48.04°, 53.89°, 55.05°, 62.69°, and 68.77° match with the (101), (004), (200), (105), (211), (204), and (116) planes, respectively, consistent with JCPDS card no. 21-1272. The tetragonal structure was observed and it belongs to the space group I41/amd (#141). Diffraction peaks for TiO_2 NPs before annealing (black line) are sharper and more intense**,** especially at (101) plane, indicating better crystallinity. After annealing (red line), the peak intensity decreases slightly and becomes broader, or particle agglomeration during annealing as the heat treatment allows nanoparticles to merge, increasing crystallite size but sometimes reducing diffraction intensity[6]. No rutile phase or impurity peaks were observed before or after annealing confirming the stability of the anatase phase. Using the Debye-Scherrer equation, the average crystallite size and dislocation line density were also calculated[7]**.**

$$D = \frac{K\lambda}{\beta COS\ \theta} \qquad (4)$$

where D is the average crystallite size, k denotes the shape factor (generally accepted as 0.9), λ signifies the wavelength of the X-ray (1.5406 Å), β indicates the full width at half maximum (FWHM) of the most prominent diffraction peak, and θ refers to the Bragg angle. The dislocation line density (**δ**) of TiO_2 NPs was calculated as

$$\delta = \frac{1}{D^2} \qquad (5)$$

The average crystallite size decreased from 4.75 nm before annealing to 3.69 nm after annealing, while the dislocation density increased from 0.01×10^{15} to 0.245×10^{15} lines/m².The increase in dislocation density suggests that defects were generated during annealing, which could impact their optoelectronic properties.

3.2. Raman analysis

Raman spectra were recorded to analyze structural changes, as shown in Figure 2(b). Raman analysis showed a prominent Eg(1) mode at 144 cm^{-1}, which is indicative of the anatase phase and corresponds to the symmetric stretching vibrations of oxygen atoms in the O–Ti–O bonds, while the A1g mode, arising from anti-symmetric bending is also present. Additional Raman peak, corresponding to overlapping (A_{1g} + B_{1g}) modes around 515 cm^{-1} and an $E_g(3)$ mode near 640 $cm^{-1}$was observed, further confirming the presence of anatase phase[8].These vibrational features are consistent with the tetragonal crystal structure (space group $I4_1/amd$) and align well with the XRD results. Before annealing, the Raman peaks most notably $E_g(1)$ around 144 cm^{-1} are sharp and intense, indicating well-developed anatase phase. After annealing, these peaks become weaker and slightly broadened, suggesting grain growth and reduced phonon confinement, which can cause decreased vibrational intensity and band broadening [9]**.** Figure 2(a) and (b) show the XRD and Raman results of 2 h TiO_2 before and after annealing, respectively

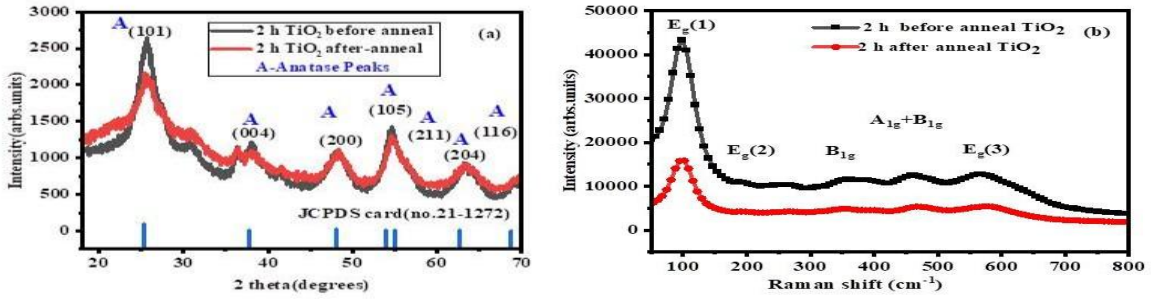

Figure 2: (a) XRD patterns and (b) Raman spectra of TiO_2 nanoparticles.

3.3 Scanning Electron Microscopy **(**SEM) Analysis

SEM images of TiO_2 NPs before and after annealing are shown in the Figure.3 (a and b)**.** The unannealed sample exhibits irregular, loosely packed particles with noticeable agglomeration and porosity. After annealing, the particles become more defined and densely packed**,** suggesting improved crystallinity and slight grain growth due to thermal treatment [10]. The limited stirring time leads to moderate uniformity, but annealing helps enhance the particle structure.

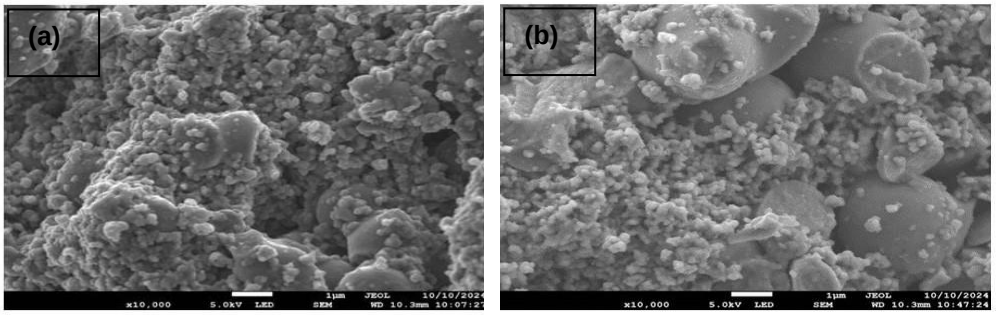

Figure 3: SEM images of TiO_2 nanoparticles (a) Unannealed and (b) annealed for 2 hr.

3.4. Diffuse Reflectance Spectroscopy (DRS) UV–Vis Analysis

Figure 4(a) and (b): UV–Vis DRS results and band gap energy of TiO_2 before and after annealing. The optical characteristics of TiO_2 NPs were analyzed using DRS UV–Vis in the 200–700 nm range, as shown in Figure 4(a). The spectra exhibited an absorption edge shift from around 390 nm before annealing to approximately 450 nm after annealing, indicating the photon absorption of TiO_2 NPs in the UV range. This shift suggests enhanced crystallinity and reduced surface defects. The band gap values were estimated from Tauc plots using the Kubelka–Munk function F(R), revealing a slight band gap narrowing after annealing, as shown in Figure 4(b).

$$F(R) = \frac{(1-\mathrm{R})^{1/2}}{2(\mathrm{R})} \qquad (6)$$

where the Kubelka-Munk function is denoted by F(R).Tauc plots were used to measure the optical band gap of TiO_2 NPs [$(F(R)hv)^{1/2}$ vs. hv], which showed an indirect transition[11].The band gap decreased from 2.85 eV before annealing to 2.73 eVafter annealing. The decrease in band gap after annealing is attributed to increased particle size, reduced surface defects, and the formation of oxygen vacancies that introduce deep-level states within the band gap [12].

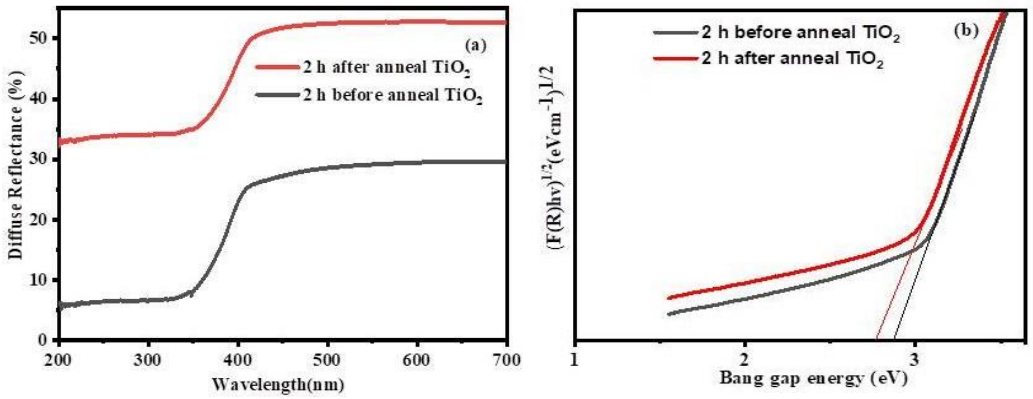

Figure 4: (a): UV–Vis spectra and (b) estimated band gap energy of TiO_2 nanoparticles, unannealed and annealed at 2 hr.

3.5 SCAPS-1D Simulation

The photovoltaic performance of the $CH_3NH_3PbI_3$-based PSC was assessed using SCAPS-1D simulation, with the electron transport layer (ETL) being experimentally set as TiO_2 NPs. The simulated device structure (ITO/TiO_2/$CH_3NH_3PbI_3$/SpiroOMeTAD/Au) showed PCE of 25.71% for TiO_2 NPs before annealing and 24.42% after annealing. This slight decrease after annealing correlates with the experimental data, where annealing improved crystallinity and purity but may have introduced slight agglomeration, affecting charge transport. The current–voltage (J–V) curves further support this trend by showing reduced current density after annealing, indicating changes in charge collection as shown in Figure 5[13]. Overall, the simulation confirms that TiO_2 NPs in the anatase phase offer a highly effective ETL, balancing structural and optical properties for efficient solar cell operation. Table 1 shows the input parameters for SCAPS-1D and Table 2 gives the simulation results[14].

Table 1: Simulation parameters for the proposed perovskite device configuration.

Device Parameters	ITO (Indium Tin Oxide) [14]	Before annealing 2 hr TiO_2 (ETL) [Own work]	After annealing 2 hr TiO_2 (HTL) (ETL) [Own work]	$CH_3NH_3PbI_3$ (Perovskite) [14]	Spiro-OMeTAD [14]
T(nm)	5	30	30	700	200
Eg (eV)	3.5	2.85	2.73	1.6	3.0
χ (eV)	4	4	4	4	2.45
εr	9	9	9	9	3
Nc (cm^{-3})	2.2 x10^{18}	2 x10^{18}	2.2 x10^{18}	2.2 x10^{18}	2.2 x10^{18}
Nv (cm^{-3})	1.8 x10^{18}	1.8 x10^{19}	1.8 x10^{19}	2.2x10^{19}	1.9 x10^{19}
μn ($cm^{-2}V^{-1}S^{-1}$)	30	20	20	2.0	2 x10^{-4}
μp ($cm^{-2}V^{-1}S^{-1}$)	5	10	10	2.0	2 x10^{-4}
Ev (cm/s)	1 x10^{7}	1 x10^{7}	1 x10^{7}	1 x10^{7}	1 x10^{7}
hv (cm/s)	1 x10^{7}	1 x10^{7}	1 x10^{7}	1 x10^{7}	1 x10^{7}
NA (cm^{-3})	0	0	0	1 x10^{13}	1 x10^{18}
ND (cm^{-3})	2 x10^{20}	1 x10^{16}	1 x10^{16}	0	0

Table 2: SCAPS-1D simulated results of the proposed proposed perovskite device configuration.

Sample	V_0(V)	(Jsc) mA/cm^2	(FF)%	(PCE) %
TiO_2 Unannealed	1.3400	23.606397	81.28	25.71
TiO_2 Annealed	1.3348	23.582969	77.58	24.42

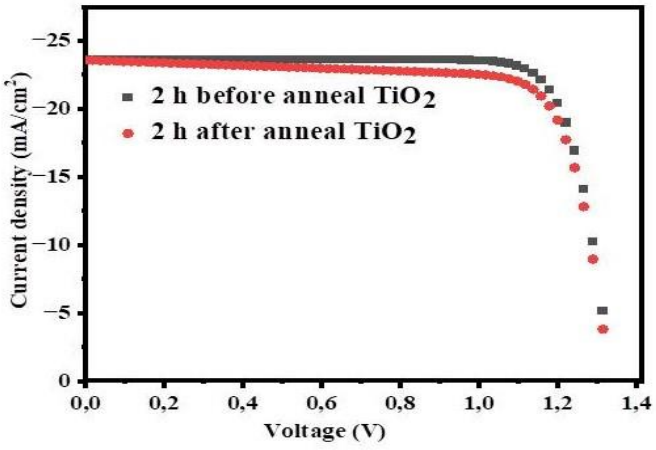

Figure 5: Simulated current density vs voltage spectra for the proposed perovskite device configuration.

4. Conclusion

In this work, TiO_2 NPs synthesized via the sol–gel method and annealed at 500 °C for 3 h showed significant structural and optical improvements. XRD and Raman analysis confirmed the anatase phase with enhanced crystallinity after annealing. SEM revealed better particle uniformity, while UV–Vis results indicated a slight band gap reduction due to increased particle size. SCAPS-1D simulations have shown that these improvements can possibly have a positive impact on the performance of $CH_3NH_3PbI_3$-based perovskite solar cells. These results demonstrate that TiO_2 NPs are suitable material as a light traping and an ETL for improving the performance and stability of $CH_3NH_3PbI_3$-based perovskite solar cells.

5. Acknowledgements

We gratefully acknowledge the use of SCAPS-1D for our simulations and the University of South Africa for funding this study.

References

[1] E. Danladi *et al.*, "20.730% highly efficient lead-free CsSnI3-based perovskite solar cells with various charge transport materials: a SCAPS-1D study," *Multiscale and Multidisciplinary Modeling, Experiments and Design,* vol. 8, no. 1, pp. 1-21, 2025.

[2] M. Baro and P. Borgohain, "SCAPS-1D device simulation of highly efficient perovskite solar cells using diverse charge transport layers," *Journal of Electronic Materials,* vol. 52, no. 11, pp. 7623-7644, 2023.

[3] K. Santhi, M. Navaneethan, S. Harish, S. Ponnusamy, and C. Muthamizhchelvan, "Synthesis and characterization of TiO2 nanorods by hydrothermal method with different pH conditions and their photocatalytic activity," *Applied Surface Science,* vol. 500, p. 144058, 2020.

[4] M. K. Hossain *et al.*, "Numerical analysis in DFT and SCAPS-1D on the influence of different charge transport layers of CsPbBr3 perovskite solar cells," *Energy & Fuels,* vol. 37, no. 8, pp. 6078-6098, 2023.

[5] A. Usman and T. Bovornratanaraks, "Modeling and Optimization of Modified TiO2 with Aluminum and Magnesium as ETL in MAPbI3 Perovskite Solar Cells: SCAPS 1D Frameworks," *ACS omega,* vol. 9, no. 38, pp. 39663-39672, 2024.

[6] Z. S. Khalifa, "Grain size reduction on nanostructured TiO 2 thin films due to annealing," *RSC Advances,* vol. 7, no. 48, pp. 30295-30302, 2017.

[7] R. Jaffar *et al.*, "Structural, optical, dielectric and photovoltaic properties of Sn doped CdS films prepared with green synthesis route," *Optical Materials,* vol. 133, p. 112964, 2022.

[8] F. Tian, Y. Zhang, J. Zhang, and C. Pan, "Raman spectroscopy: a new approach to measure the percentage of anatase TiO2 exposed (001) facets," *The Journal of Physical Chemistry C,* vol. 116, no. 13, pp. 7515-7519, 2012.

[9] X. Wang, G. Wu, B. Zhou, and J. Shen, "Thermal annealing effect on optical properties of binary TiO2-SiO2 sol-gel coatings," *Materials,* vol. 6, no. 1, pp. 76-84, 2012.

[10] L. Wang, Z. Li, T. Itoi, H. Yoshida, and Y. Lu, "Grain growth and phase transformation of nano-sized titanium dioxide powder during heat treatment and spark plasma sintering," *journal of materials research and technology,* vol. 20, pp. 4409-4418, 2022.

[11] P. Anilkumar, T. Kalaivani, S. Deepak, J. Jasmin, and A. E.-R. AF, "Evaluation of structural, optical and morphological properties of La doped TiO2 nanoparticles," *Ceramics International,* vol. 49, no. 11, pp. 16991-16998, 2023.

[12] S. Mohamed and A. A. Alhazime, "Suppressing photoluminescence and enhancing light absorption of TiO2 via using TiO2/TiN/TiO2 plasmonic multilayers for better solar harvesting," *Journal of Materials Research and Technology,* vol. 18, pp. 4470-4478, 2022.

[13] C. Son, H. Son, and B.-S. Jeong, "Enhanced conversion efficiency in MAPbI3 perovskite solar cells through parameters optimization via SCAPS-1D simulation," *Applied Sciences,* vol. 14, no. 6, p. 2390, 2024.

[14] E. Danladi *et al.*, "20.730% highly efficient lead-free CsSnI3-based perovskite solar cells with various charge transport materials: a SCAPS-1D study," *Multiscale and Multidisciplinary Modeling, Experiments and Design,* vol. 8, no. 1, p. 114, 2025.